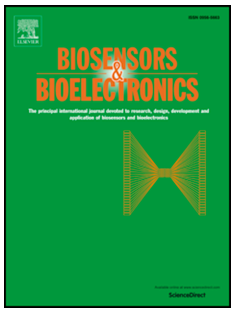

Clinically comparable impedimetric immunosensor for serum alkaline phosphatase detection based on electrochemically engineered Au-nano-dendroids and graphene oxide nanocomposite

Kuldeep Mahato, Buddhadev Purohit, Ashutosh Kumar, Pranjal Chandra

PII: S0956-5663(19)30894-2

DOI: https://doi.org/10.1016/j.bios.2019.111815

Reference: BIOS 111815

To appear in: *Biosensors and Bioelectronics*

Received Date: 26 August 2019

Revised Date: 15 October 2019

Accepted Date: 22 October 2019

Please cite this article as: Mahato, K., Purohit, B., Kumar, A., Chandra, P., Clinically comparable impedimetric immunosensor for serum alkaline phosphatase detection based on electrochemically engineered Au-nano-dendroids and graphene oxide nanocomposite, *Biosensors and Bioelectronics* (2019), doi: https://doi.org/10.1016/j.bios.2019.111815.

Conceptualization; KM, PC

Data curation; KM, PC

Formal analysis; KM, AK, BP, PC

Funding acquisition; PC

Investigation; KM, AK, BP, PC

Methodology; KM, PC

Project administration; PC

Resources; PC

Software; IIT G

Supervision; PC

Validation; KM, PC

Visualization; KM, PC

Roles/Writing - original draft; KM, PC

Writing - review & editing. KM, AK, BP, PC

Clinically comparable impedimetric immunosensor for serum alkaline phosphatase detection based on electrochemically engineered Au-nano-Dendroids and Graphene Oxide nanocomposite

Kuldeep Mahato, Buddhadev Purohit, Ashutosh Kumar, Pranjal Chandra *

Laboratory of Bio-Physio Sensors and Nano-bioengineering,
Department of Bioscience and Bioengineering, Indian Institute of Technology Guwahati,
Guwahati-781039, India

*Corresponding author

Pranjal Chandra, Ph.D.
Laboratory of Bio-Physio Sensors and Nano-bioengineering,
Department of Bioscience and Bioengineering,
Indian Institute of Technology Guwahati, Guwahati-781039, India
Email: pchandra13@iitg.ac.in, pranjalchandra13@gmail.com
Phone: +91361-2583207; Fax: +91361-258-2249

Abstract:

In this work, we demonstrate label-free electrochemical impedance spectroscopy (EIS) based alkaline phosphatase (ALP) detection using gold nanoparticles (AuNPs), electrochemically engineered Au-nano-Dendroids, and graphene oxide (GO) nanocomposite. These nanomaterials were sequentially deposited on to the screen-printed carbon electrode (SPCE) and antibodies against ALP (anti-ALP) were immobilized using carbodiimide bioconjugation process. The sensor probe has been characterized extensively using TEM, EDX, SAED, XRD, FE-SEM, FTIR, DIC, and electrochemical techniques. The analytical performance of fabricated biosensor has been evaluated using EIS, where linear dynamic range and limit of detection were obtained to be 100-1000 U/L and 9.10 (±0.12) U/L, respectively. The developed biosensor showed high selectivity towards ALP with negligible interference (k_{sel} << 1; n=3) due to coexisting molecules. The sensor probe has successfully recovered ALP between 108.84% and 172.50% (n=3) in human serum samples. The sensor has been used to estimate ALP in clinical serum samples, where the level was found to be 83.15 U/L and was comparable with standard technique used in the hospitals. The shelf life, stability, and reproducibility have been also been evaluated.

Keywords: Human Health; Alkaline Phosphatase; Immunosensor; Dendroids; Clinical Validation

1. Introduction:

ALP is a phosphate-cleaving enzyme found in biofluids (viz. serum, saliva, and other bodily secretions) and participates in various vital physiological functions in biological systems. The physiological range of serum ALP in adults is 20-140 U/L in the case of a normal adult, which increased slightly higher in case of infants, kids, and pregnant women. The clinical ranges above 350 U/L were reported in case of liver and bone associated disorders. Moreover, elevated serum ALP level is also found in various cases of cancer relapse (Buonaguro et al., 2019) and at the onset of hepatitis C (Bodlaj et al., 2010; Keshaviah et al., 2007). In current clinical scenario, the serological determinations of ALP are performed using the method reported by McComb and coworkers, where ALP can be detected by formation of a chromogenic product (p-nitrophenol) (McComb and Bowers, 1972). This chromogenic product is formed due to ALP transphosphorylation capability. Inspired by these spectroscopic methods, various other methods have also been reported to detect ALP using wide range of substrates, *viz*. 5-Bromo-4-chloro-3-indolyl phosphate (BCIP) (Xi et al., 2016), nitro blue tetrazolium (Takehana et al., 2019), 4-Aminophenylphosphate *etc* (Jiang et al., 2016). In addition to the colorimetric detection of ALP in blood serum, chemiluminescence, fluorescence, and surface-enhanced Raman spectroscopy based sensing have also been tested (Hallaway and O'Kane, 2000; Kim et al., 2011; Ruan et al., 2006). Moreover, electrochemical based techniques (*viz.* voltammetry , amperometry, *etc*.) are used for the detection of ALP in recent past, where the product formed after ALP catalysis has been targeted for its quantification (Lee et al., 2018; Wang et al., 2009). These reported methods have used the indirect approach to detect ALP as well as involves multiple enzymes, which eventually arises complexity and non-robustness. Furthermore, these sensors are susceptible to the insensitive, false positive response especially in real sample environments due to the certain coexistences of other peroxidases and redox active molecules (King and Delory, 1948).

In recent past, the advances in nano-fabrication have paved a way to obtain robust biosensors for the direct sensing of bio-analytes (Chandra, 2016; Chandra et al., 2017), where various metallic nanocomposite (Pei et al., 2015; Zhao et al., 2016; Zhao et al., 2015) have been used by exploiting their excellent optoelectronic properties (Baranwal et al., 2016; Mahato et al., 2019). Recently,

branched-metallic structures-based nanocomposite have been employed in various applications including energy storage and nano-catalysis. These structures have also been attempted in various biosensing methods because of relatively larger surface area for the electron conduction at sensor surfaces (Valera et al., 2019), which eventually contributes sensitive determination. However, most of the reported biosensors using metallic dendrites follow direct electrochemical transfer method, where the target analyte participates in electro-catalysis at the sensor surface to generate electrochemical signals. Few works have also been reported by immobilizing the recognition elements by physical adsorption on these nanostructures (Fu et al., 2017; Wang et al., 2018), which are considered to be unstable due to its susceptibility of leaching out. Therefore, these metallic branch-structured nanomaterials are limited when there is a need for stable coupling of bio-receptors due to absence of the flanking groups, which are used for covalent immobilization. Thus, branched structure-based nanocomposite has been used for coupling the bio-receptors by incorporating additional materials comprising flanking functional groups. In one of these strategies the composite consisting of branched Au-metallic-structure and conducting polymers of poly-pyrrole has been used to immobilize the antibody (Valera et al., 2019), which may suffer for less sensitivity caused by loss of conductivity due to disruption of molecular planarity in presence of added functional groups during functionalization (Berezhetska et al., 2015; Jimison et al., 2012). To overcome such limitations, GO has been used in sensor matrix due to the excellent availability of flanking groups for covalent immobilization. To the best of our knowledge this combination has never been utilized to immobilize bioreceptor for immuno-sensors. Therefore, it is interesting to attempt such kind of new matrices in sensitive sensor fabrication.

In view of such importance, we demonstrate a direct label-free immunosensor for serum ALP detection on the Au-branched structures (Au-nano-Dendroids) and GO nanocomposite based biosensing probe. The biosensor has been developed on an SPCE by sequential deposition of nanomaterials (*viz.* AuNPs, Au-nano-Dendroids, GO sheets) and immobilization of anti-ALP bioreceptor. Followed by this, the fabricated SPCE/AuNPs/Au-nano-Dendroids/GO/anti-ALP biosensor has been characterized systematically using Fourier transformed infrared spectroscopy (FTIR), field emission scanning electron microscopy (FE-SEM), transmission electron microscopy

(TEM), energy-dispersive X-ray spectroscopy (EDX), selected area electron diffraction (SAED), and X-Ray diffraction (XRD), linear sweep voltammetry (LSV), EIS, and digital image colorimetry (DIC). The analytical performance of biosensor has been evaluated using EIS in the spectral range of 10^6 to 10 Hz. The interferences due to coexisting molecules have also been evaluated. The sensor probe has been tested in blood serum samples to assess the analytical capability in clinical samples using spike-recovery and standard addition methods. The unknown concentration of ALP in serum sample has also been evaluated using standard addition method, which was found to be comparable with clinical method. The shelf life of fabricated SPCE/AuNPs/Au-nano-Dendroids/GO/anti-ALP probe has also been evaluated.

2. Experimental:

2.1. Chemicals and instrumentation:

The chemicals and instruments used in the experiment have been detailed in the **SI-1** of supplementary information.

2.2. Synthesis of GO:

For the synthesis of GO, modified Hummer's method was adopted (Zaaba et al., 2017). The brief discussion on adopted synthetic procedure has been described in **SI-2** of supplementary information.

2.3. DIC-based control study:

For the DIC based study, 50 µL of 5 mM BCIP solution was employed onto the final probe after immuno-complexation at working electrode region. The captured ALP catalyzes BCIP to a blueish green colored compound 5,5'-dibromo-4,4'-dichloro-indigo. The incubation time for BCIP on to the immuno-complexed sensor probe has been optimized by using DIC techniques, where incubation time for colored product formation from BCIP is found optimum at 30 minutes. The process of optimization has been described in section **SI-3** of supplementary section. **Figure SI-1 (A-B)** shows the time-dependent imaging of ALP immuno-complexed SPCE/AuNPs/Au-nano-Dendroids/GO/anti-ALP sensor chip after incubation of 50 µL of BCIP and the obtained plot after DIC analysis using the captured images. Thus, by keeping BCIP solution for 30 minutes over the working electrode, the colored solution has been taken to the hydrophobic cellulose acetate thin sheet with a white

background and appeared color was captured using smartphone camera. Thereafter, the captured image was processed using RGB (Red, Green, and Blue) profiler application at the droplet region and values were extracted to trace the color change. Further, DIC analysis in the control studies was also performed using the procedure followed by the technique reported earlier (Mahato and Chandra, 2019). Briefly, effective normalized intensities corresponding to the color change were obtained using equation 1.

$$Effective\ I_{\mathrm{Red}} = \log_{10}\left(\frac{I_{\mathrm{Red}\ (Blank)}}{I_{\mathrm{Red}\ (Conc.)}}\right) \text{---------- Equation 1}$$

Where I_{Red} is the mean pixel intensity of the red channel, which is obtained from selected area analyses.

2.4. SPCE/AuNPs/Au-nano-Dendroids/GO/anti-ALP Sensor probe fabrication:

The sensor probe has been fabricated by sequential surface modifications on to the bare SPCE. In the first step, SPCE has been modified with electrochemically deposited AuNPs. In this step, the AuNPs were deposited electrochemically on to the bare SPCE, where acidic solution of $HAuCl_4$ (0.005% in 0.5M H_2SO_4) was taken as an electrolyte in three-electrode system and allowed for consecutive five LSV scans under the potential window of 1.5 V to 0.4 V at the scan rate of 100 mV/s. The provided voltage and time for deposition of -0.6 V and 60 seconds, respectively. In the next step, Au-nano-Dendroids were synthesized electrochemically on to the SPCE/AuNPs modified surface. The deposition of Au-nano-Dendroids ware achieved by the electrochemical deposition process, where chrono-amperometric technique was employed, which has been performed at - 0.3 V for 600s using the three-electrode system containing $HAuCl_4$ solution (5% in KCl 0.1M) as an electrolyte. In the further step, synthesized GO has been coated onto the SPCE/AuNPs/Au-nano-Dendroids modified electrode surface. Briefly, GO solution (1mg/mL) was prepared by dissolving GO in ethanol and coated 2 µL of the solution by spin coating method followed by 30 minutes of drying. The dried SPCE/AuNPs/Au-nano-Dendroids /GO electrode surface was then activated for the anti-ALP immobilization. For that, 50 microliters of the solution containing ethyl(dimethylaminopropyl) carbodiimide - N-hydroxysuccinimide (EDC-NHS; 100 mM-100 mM) was treated and incubated for 30 minutes (Roy et al., 2011). After this incubation, the EDC-NHS was

washed and 4 microliters of anti-ALP (pH 7.0) were treated with SPCE/AuNPs/Au-nano-Dendroids /GO modified surface for 30 minutes which was found to be optimum time for anti-ALP immobilization **(Figure SI-2 (A-B))**. The detailed optimization process has been described in the SI-4 section of the supplementary information. After incubation, the sensor probe surface was gently washed with distilled water to remove unreacted anti-ALP followed by the 0.1% bovine serum albumin blocking for nullifying nonspecific interaction sites. The final modified sensor probe was termed as SPCE/AuNPs/Au-nano-Dendroids/GO/anti-ALP. The step by step sensor probe fabrication and detection principle have been shown in **scheme 1**.

3. Result and discussions:

3.1. Characterization of GO:

After the successful synthesis of GO using the modified hammers method, it has been systematically characterized using the TEM, EDX, SAED, and XRD techniques. In the first step, GO was exfoliated before the TEM imaging, where clear transparent sheet was observed, indicating the successful synthesis of the graphene sheets (**figure 1(A)**). In the following step, to know elemental composition of the graphene sheets EDX has been recorded (**figure 1(B)**), where the clear elemental composition of C and O has been obtained, which indicates the sheets consisting the GO. Thereafter, the material properties of GO have been studied using SAED and XRD, where clear SAED ring pattern (**figure 1(C)**) and the peak in X-ray diffractograms (**figure 1(D)**) shows crystalline nature of the material.

3.2. SPCE/AuNPs/ Au-nano-Dendroids /GO/anti-ALP sensor probe characterization:

The fabrication of SPCE/AuNPs/Au-nano-Dendroids/GO/anti-ALP sensor probe has been characterized using the physical as well as electrochemical techniques *viz.* FE-SEM, FTIR, LSV, and EIS have been used. Firstly, the fabrication process has been assessed by FE-SEM, where the surface topological changes have been analyzed. For this, the FE-SEM micrographs of the bare electrode surface, AuNPs deposited electrode surface, dendroids synthesized AuNPs deposited electrode surface, GO deposited on the dendroids grown electrode surface, and anti-ALP immobilized at the GO modified electrode surface was captured (**figure 2(A)**). From the figure, clear small bright uniform dot imprints have been observed at the AuNPs deposited electrode surface **(ii),** which was,

however, not observed at the bare electrode surface **(i).** This indicates the successful deposition of AuNPs on to bare electrode surface. In next micrograph, a layer of irregular protruded features at modified surface was observed at **(iii – iii"),** indicating the deposition of dendroids like Au-nanostructures. Thereafter, in the micrograph next to this **(iv – iv"),** patches of small flakes were observed over Au-nano-Dendroids deposited surface, indicating the successful deposition of GO over previously modified surface. At the final step of modification, EDC-NHS has been treated to immobilize anti-ALP. The FE-SEM micrograph recorded after immobilization of anti-ALP **(v – v")** shows clear change in surface topology with granular structure, indicating the successful anti-ALP immobilization.

In order to confirm such modification at the sensor surface, corresponding FTIR spectra **(figure 2(B))** at bare SPCE, SPCE/AuNPs, SPCE/AuNPs/Au-nano-Dendroids, SPCE/AuNPs/Au-nano-Dendroids/GO, and SPCE/AuNPs/Au-nano-Dendroids/GO/anti-ALP modified surfaces. In the FTIR spectrum corresponding to bare SPCE, peaks at 3255 cm^{-1} and 1065 cm^{-1} were observed. These correspond to -OH and C-C stretching vibrations, which are present in the carbon paste and used binder in SPCE. In the spectrum taken after SPCE/AuNPs, the peaks were observed much fainted which is due to the deposition of AuNPs over SPCE. Not only in this step, the peaks completely disappeared in next step of modification, where Au-nano-Dendroids were electrochemically grown which is due to the further metallic layering over the exposed SPCE surface. This layering of Au-nano-Dendroids can also prominently be visualized by naked eye, where the color of SPCE surface changes from dark black to golden brown color. In the next spectrum, the appearance of peaks at 3253 cm^{-1}, 1645 cm^{-1}, 1420 $cm^{-1,}$ and 1065 cm^{-1} were observed, which are due to the –OH, C=O, C-OH, and C-C vibrations of GO confirming the successful deposition of the GO at SPCE/AuNPs/Au-nano-Dendroids electrode surface. The appearance of new vibrational peaks along with a subtle shift has been observed in the next spectrum at anti-ALP immobilized SPCE/AuNPs/Au-nano-Dendroids/GO surface, where the broad peak at the 3253 cm^{-1} was found narrower and appearance of a new peak at 1558 (amide I) cm^{-1} was observed. In addition to this, the slight shift of –C=O peak at 1635 cm^{-1} (amide II) and 974 cm^{-1} (C-C-C) were found, indicating the successful immobilization of anti-ALP at the GO flakes.

Thereafter, in order to assess the charge transfer behavior of fabricated SPCE/AuNPs/Au-nano-Dendroids/GO/anti-ALP probe, we have characterized the fabrication process using electrochemical techniques. The deposition of AuNPs was characterized using the LSV technique where consecutive scans were performed. The clear reduction peak at 0.95 (V) vs. Ag/AgCl was observed. This reduction peak is due to the reduction of Au^{3+} of solution phase to Au^0 at the electrode surface, which eventually forms AuNPs at SPCE electrode surface (**figure SI-3 (A)**). Interestingly, when the subsequent scans were performed, the increment on reduction peak was observed, indicating its gradual increment in charge transfer and enhanced conductivity of modified surface. In the subsequent step, nano-dendroids like structures have been grown onto the SPCE/AuNPs modified electrode surface using chrono-amperometric technique. **Figure SI-3(B)** shows the chorno-amperometric response due to the deposition of Au^0 at electrode surface eventually deposits nano-Dendroids, the gradual increment of current, in the beginning, is due to the increased conductivity of surface. After few seconds, the amperometric response attained its plateau, indicating the initiation of Au-nano-Dendroids formation over the SPCE/AuNPs modified surface. On further continuation, the current response was observed constant at plateau level, indicating the vertical growth of the Au-nano-Dendroids **(figure SI-3(B)).**

In the next step, the modified electrode was assessed by recording LSV under the experimental conditions of the window -0.2 V to 0.6 V at a scan rate of 50 mV/s in 5mM Zobell's solution. **Figure 3(A)** shows the LSV responses for bare SPCE (black), SPCE/AuNPs (red), SPCE/AuNPs/Au-nano-Dendroids (blue), SPCE/AuNPs/Au-nano-Dendroids/GO (grey), and SPCE/AuNPs/Au-nano-Dendroids/GO/anti-ALP (pink). The representative peak currents (I_{pa}) were observed at the 0.26 V due to the electrochemical behavior of the mediator. It is interesting to note that the anodic peak current was found to be increased when SPCE/AuNPs were analyzed. This increment is due to the deposition of AuNPs over SPCE surface, making the surface conducting as well as increasing effective surface area for charge transfer. Thereafter, Au-nano-Dendroids were deposited over the SPCE/AuNPs surface, the LSV response has been observed with further increments in the peak current, indicating the SPCE/AuNPs/Au-nano-Dendroids modified surface is capable of giving amplified signal. This amplification of signal is due to the further increment of the

surface area for charge transfer and its conducting behavior. In next step, GO was deposited over the previously modified electrode surface and the LSV has been recorded at SPCE/AuNPs/ Au-nano-Dendroids/GO surface and peak currents were analyzed. The effective current was decreased due to less conducting behavior of GO. In further step of probe fabrication, anti-ALP was conjugated using the EDC-NHS bio-conjugation technique over the SPCE/AuNPs/Au-nano-Dendroids/GO modified surface and the LSV was recorded. The effective peak currents were found to be decreased in these modified electrodes, which is due to the insulating nature of anti-ALP. Finally, the fabricated sensing probe was termed as SPCE/AuNPs/Au-nano-Dendroids/GO/anti-ALP. We have also tested other combinations (SPCE/AuNPs/Au-nano-Dendroids/GO/anti-ALP, SPCE/AuNPs/GO/anti-ALP, SPCE/Au-nano-Dendroids/GO/anti-ALP and SPCE/GO/anti-ALP) to show the importance of nanomaterials towards signal amplification. Among the tested probes maximum current was observed in case of SPCE/AuNPs/Au-nano-Dendroids/GO/anti-ALP (**figure SI-4**), indicating that incorporation of AuNPs and Au-nano-Dendroids has amplified the signal greatly. The electrochemical behavior of any fabricated surface depends on the charge transfer phenomena occurring at electrode/electrolyte interface, where the diffusion of charge carriers plays an important role in electrochemical sensing. In order to assess the importance of modified surfaces for charge transfer capability in such phenomenon, we have deduced the diffusion coefficients of bare SPCE and every layer of the modified electrode using Randles-Sevick's model (Equation - 2) and found 1.5-fold greater transfer of charge species through SPCE/AuNPs/Au-nano-Dendroids/GO/anti-ALP modified electrode surface than the bare SPCE.

$$I_p = \left(2.69\times10^5\right) n^{3/2} ACD^{1/2} v^{1/2} \quad \text{…….. Equation 2}$$

Where, I_p is the peak current (in ampere), n is number of electrons transferred in redox process (here n=1), A is the electrode surface area (in cm^2: here A = 0.196 cm^2), C is the concentration of electroactive species (in mole cm^{-3}), D is the diffusion coefficient (in $cm^2\ s^{-1}$), and v is the scan rate (in $V\ s^{-1}$).

The findings of Randles-Sevcik's model clearly suggest that developed SPCE/AuNPs/Au-nano-Dendroids/GO/anti-ALP sensing surface is relatively conducting and capable of transferring

greater amount of charged species in order to provide better sensitivity. The results obtained by LSV were also validated using EIS, where spectra in the Nyquist plot were recorded for bare SPCE (black), SPCE/AuNPs (red), SPCE/AuNPs/Au-nano-Dendroids (blue), SPCE/AuNPs/Au-nano-Dendroids/GO (grey), and SPCE/AuNPs/Au-nano-Dendroids/GO/anti-ALP (pink) surfaces to obtain the resistance in charge transfer (R_{ct}) (**Figure 3(B)**). The obtained R_{ct} values were 381.13±2.92, 352.71±2.72, 311.13±2.42, 316.36±2.46, and 331.81±2.58 for the bare SPCE (black), SPCE/AuNPs (red), SPCE/AuNPs/Au-nano-Dendroids (blue), SPCE/AuNPs/Au-nano-Dendroids/GO-Naf (grey), and SPCE/AuNPs/Au-nano-Dendroids/GO/anti-ALP (pink) surfaces, respectively (**Figure 3(B); inset**). These results confirm that the developed SPCE/AuNPs/Au-nano-Dendroids/GO/anti-ALP probe is capable of delivering sensitive detection; hence, it is suitable for electrochemical analysis. In order to assess process involved at the electrode/electrolyte interface, scan rate study has been performed, where the LSV at SPCE/AuNPs/Au-nano-Dendroids/GO/anti-ALP sensor probe has been recorded with varying scan rates between 10-100 mV/s (shown in **figure 3(C)**). Thereafter, the scan rate dependent plot is obtained, where peak currents were plotted against the square root of scan rates **(figure 3(D))**. The linear relationship between current and square root of scan rates clearly suggests that the involvement of the diffusion-controlled process at the electrode/electrolyte interface. The continuous increment of peak currents with the scan rate also indicates the stable fabrication of probe, which otherwise could be nonlinear increment with increasing scan rates.

3.3. Control studies for the SPCE/AuNPs/Au-nano-Dendroids/GO/anti-ALP sensor probe:

Before assessing the analytical performance of designed SPCE/AuNPs/Au-nano-Dendroids/GO/anti-ALP sensor probe, its immuno-complexation ability with ALP was confirmed. For that, the droplet assisted DIC based technique has been employed by exploiting the catalytic activity of ALP. To do so, the sensor and control probes have been incubated with 50 µL of 5 mM BCIP solution, which is a substrate for the ALP and gives the blue-green colored complex (**figure 4(A)**). **Figure 4(B)** shows the effective intensities correspond to **(i)** SPCE/AuNPs/Au-nano-Dendroids/GO/ALP, **(ii)** SPCE/AuNPs/Au-nano-Dendroids/GO/anti-ALP/, and **(iii)** SPCE/AuNPs/Au-nano-Dendroids/GO/anti-ALP/ALP surfaces, where the blocking agent was treated post to the EDC-NHS activation (in case of **(i)**) / antibody immobilization (in case of **(ii-iii)**) in every

probe to avoid the nonspecific interactions. The effective intensity corresponds to SPCE/AuNPs/Au-nano-Dendroids/GO/anti-ALP/ALP surface was found to be 0.58 units, which is significantly ($p < 0.01$, n=3) higher from the controls, suggesting the successful immuno-complexation of ALP with SPCE/AuNPs/Au-nano-Dendroids/anti-ALP sensor probe and no adsorption of ALP has occurred in the fabrication process.

3.4. Analytical performance:

After the validation of ALP sensing by fabricated SPCE/AuNPs/Au-nano-Dendroids/GO/anti-ALP sensor probe, we have performed the dose-dependent study for assessing its analytical performance, where the dosage of different concentrations of ALP was treated to fabricated sensor. Briefly, the sensor probe was incubated with the different concentrations of ALP for 30.0 minutes (optimized) followed by gentle rinsing of probe using sterile phosphate-buffered saline (PBS) solution and EIS have been recorded using Zobell's solution (pH-7.0 mM, 5 mM). **Figure 4(C)** shows the characteristics EIS responses of the SPCE/AuNPs/Au-nano-Dendroids/GO/anti-ALP before binding, which were found to be increased with the increasing concentration of ALP. This gradual increment of the R_{ct} is contributed by ALP immuno-complexation, which eventually introduces insulating layer to charge transfer, where the R_{ct} values were increased in Nyquist plot. A calibration plot was drown based on the R_{ct} values obtained from EIS responses in a dose-dependent study **(figure 4(D))**. The linear dynamic range was found between 100-1000 U/L. The linear regression equation is expressed as follows: R_{ct} (Ω) = 0.058 (± 0.001) [ALP] – 4.072 (± 1.117) and the limit of detection has been calculated as 9.10 (± 0.12) U/L (RSD < 3.7 %,) based on the standard deviation of three times consecutive analysis of the blank (95% confidence value, n=3). This clearly shows that the developed sensor has great potential for the detection of ALP. It is worth mentioning that the linear dynamic range of this biosensor falls within the ranges of various clinical conditions, which indicates the significance of fabricated SPCE/AuNPs/Au-nano-Dendroid/GO/anti-ALP biosensor in potential clinical diagnostics.

3.5. Selectivity assay:

To study the selectivity of fabricated SPCE/AuNPs/Au-nano-Dendroids/GO/anti-ALP biosensor probe, the assessment of sensor probe was done in presence of potentially interfering molecules found in biological fluids including serum albumin (1 mg/mL), immunoglobulin (1 mg/mL), glycine (10 mM), alanine (10 mM), glucose (10 mM), glutamic acid (10 mM), uric acid (1 mM), cysteine (10 mM), and citric acid (10mM). No interfering signals were observed from these under the tested experimental window. The selectivity of SPCE/AuNPs/Au-nano-Dendroids/GO/anti-ALP probe was mathematically deduced by determining the selectivity coefficient using the following equation 3

$$k_{sel} = \frac{(Signal)_{interferent}}{(Signal)_{ALP}} \qquad \text{---------- Equation 3}$$

Where k_{sel} *is the coefficient of selectivity,* $(Signal)_{interferent}$ *is the signal strength shown by the probe when treated with the interfering molecules, and,* $(Signal)_{ALP}$ *is the signal strength corresponds to ALP.*

The calculated k_{sel} values for interfering molecules were extremely low (k_{sel} << 1), indicating that the fabricated sensor is highly selective towards ALP (100 U/L). The results were statistically analyzed by performing the T-test of the obtained R_{ct} values, where p values were found to be << 0.001 (n = 3) for all the tested interfering molecules, indicating the selectivity results are of statistical relevance. **Figure SI-5 and Figure 5 (A)** show the EIS responses and corresponding histogram, respectively for the selectivity assay using the biosensing probe.

3.6. Real sample analysis and clinical validation:

For the commercial viability, the analytical capability of fabricated biosensor has been assessed using the real sample. Here, we have used the clinical serum sample for further assessment of the SPCE/AuNPs/Au-nano-Dendroids/GO/anti-ALP sensor probe. The whole study has been done systematically; where in the first step, the spike and recovery model were used. In this method, known

concentrations of ALP were spiked to the real sample and were recovered using fabricated sensor probe using equation 4.

$$\% \text{ Recovery} = \frac{([A]_{ALP} - [B]_{ALP})}{[C]_{ALP}} \quad \text{---------- Equation 4}$$

Where, $[A]_{ALP}$ *and* $[B]_{ALP}$ *are the analytical responses of ALP in the spiked and blank serum samples, respectively; and* $[C]_{ALP}$ *is the analytical response of* ALP *in the standard solutions.*

In this study, the dose-dependent EIS responses from the serum samples containing no ALP/ ALP were recorded using the fabricated probe, where an increase in the R_{ct} values was observed on increase in ALP concentrations. **Figure 5(B)** shows the histogram showing R_{ct} values obtained from the comparative dose-dependent responses obtained from serum sample assessments using sensor probe. The sensitivity using sensor probe was performed, where the % recovery obtained between 108.84% and 172.50% of ALP from the serum samples in various tested concentrations. The analytical details of recovered ALP, % recovery and RSD have been shown in **table 1**. The detection limit was determined which was found to be 13.15 (± 0.17) U/L (RSD < 7.8%) based on the standard deviation of consecutive five times responses of the blank (95 % confidence level, n=5). The recovered concentrations obtained in this study were observed way greater than the spiked concentration, indicating the presence of residual ALP in the serum sample. Therefore, in the next phase, we have extended the study to find the residual (unknown) concentrations of the ALP in serum sample. Here, serum samples were collected from volunteer and samples were used for ALP assessment using fabricated SPCE/AuNPs/Au-nano-Dendroids/GO/anti-ALP sensor probe and by clinical method simultaneously. For this assessment using sensor probe, standard addition method has been adopted, where the probe is first tested using five times diluted (in PBS) serum sample (no ALP spiked) and subsequent spiked known concentration of ALP followed by the recording of responses. Thereafter, standard addition plot was obtained using EIS responses, where the linear regression equation for ALP found to be R_{ct} (Ω) = 0.058 (± 0.036) [ALP] + 1.94 (± 0.677) with the correlation coefficient of 0.98. The representative standard addition plot has been shown in **figure 5(C)**, where the concentration of ALP in serum sample was calculated as 83.15 (± 2.45) U/L (RSD < 2.9 %)

(16.63 U/L x 5 dilution factor). The clinical validation of the fabricated sensor probe was done by the classical method applied in hospitals. The ALP level in the same serum sample was found to be 79.31 (± 5.0) U/L, which is comparable to the levels obtained from designed immunosensor. The concentration of ALP obtained by our sensor and routine clinical assay were comparable **(figure 5(D))**, indicating the direct clinical application of fabricated sensor in hospitals, health centers, and point of care settings.

3.7. Storage conditions, stability, and reproducibility assessment:

For studying the stability, a batch of SPCE/AuNPs/Au-nano-Dendroids/GO/anti-ALP biosensor probes were fabricated and stored at 4^{o} C. The fabricated biosensor was used to obtain the R_{ct} value after incubation with ALP in every seven days. The R_{ct} responses obtained by sensor probe shows that it retained the sensitivity of 98.13% until 56 days (shown **in figure SI-6),** while the significant decrement of signal was observed afterward, which is most likely due to the loss of biological activity of anti-ALP and/or the degradation of chemical modification steps. The considerably good shelf-life of 56 days was most likely due to the stable immobilization of anti-ALP and retention of its biological activity on SPCE sensor chip. The reproducibility of fabricated SPCE/AuNPs/Au-nano-Dendroids/GO/anti-ALP biosensor was evaluated, which showed the RSD below than the < 2.3% even when same fabrication process was followed, indicating the sensor fabrication is highly reproducible (shown in **figure SI-7**), and this variation is most likely due to the negligible deviation in the sensor fabrication steps and handling errors.

4. Conclusions:

In this present work, a biosensor for label-free detection of the serum ALP has been developed based on Au-nano-Dendroids-GO nanocomposites deposited on the SPCE. The developed sensor probe has been characterized using TEM, SAED, EDX, XRD, DIC, and electrochemical techniques. The analytical performance has been assessed, showing a dynamic range between 100 and 1000 U/L, covering the ALP levels in various pathophysiological conditions (viz. bone disease, liver disease, carcinoid syndrome, etc.) with the detection limit of 9.10 (±0.12) U/L. The biosensor is highly selective towards ALP even in the presence of various coexisting molecules including, albumin,

globulin, alanine, glucose, citric acid, uric acid, and glutamic acid (k_{sel}<< 0.08). The sensor is able to detect the ALP in clinical serum samples, which shows % recoveries between 108.84% and 172.50%. The shelf life of the biosensor has also been evaluated, where the sensor probe was found to be stable (RSD < 2.3%) up to 56 days. The fabricated biosensor has many attractive features such as robustness, easy fabrication, and its possible application in point of care analysis of serum ALP. To the best of our knowledge, this is the first work where ALP has been detected using a label-free immunosensor comprising Au-nano-Dendroids and GO-based nanocomposites in clinically comparable range and validated by standard hospital-based technique.

Figure captions:

Scheme 1: Schematic representation of the SPCE/AuNPs/ Au-nano-Dendroids/GO/anti-ALP probe fabrication or ALP determination in clinical serum sample.

Figure 1: Characterization of GO, figure shows (A) TEM micrograph (B) EDX, (C) SAED, and (D) XRD of the exfoliated GO sheet.

Figure 2: **(A)** FE-SEM micrographs of subsequently modified surfaces of **(i)** bare electrode **(ii)** AuNPs modified electrode, **(iii - iii")** Au-nano-Dendroids synthesized AuNPs modified electrode, **(iv – iv")** GO deposited on Au-nano-Dendroids modified electrode assembly, **(v – v")** anti-ALP immobilized on GO at Au-nano-Dendroids electrode modified electrode assembly. **(B)** FTIR spectra of different modified surfaces where **(i)** SPCE, **(ii)** SPCE/AuNPs, **(iii)** SPCE/AuNPs/Au-nano-Dendroids, **(iv)** SPCE/AuNPs/Au-nano-Dendroids/GO, **(vi)** SPCE/AuNPs/Au-nano-Dendroids/GO/anti-ALP.

Figure 3: LSV **(A)** and EIS **(B)** responses of the different modified electrode surfaces of SPCE **(i)**, SPCE/AuNPs **(ii)**, SPCE/AuNPs/Au-nano-Dendroids **(iii)**, SPCE/AuNPs/Au-nano-Dendroids/GO **(iv)**, SPCE/AuNPs/Au-nano-Dendroids/GO/anti-ALP **(v)** in 5mM Zobell's solution. Inset (A) and

inset (B) shows corresponding histograms obtained from the LSV and EIS responses respectively; **(C)** LSV responses of the SPCE/AuNPs/Au-nano-Dendroids/GO/anti-ALP sensor probe at different scan rates (10-100 mV/s) in Zobell's solution, **(D)** linear fit for the Ipa.

Figure 4: Control tests showing **(A)** colorimetric visual responses of (i) SPCE/AuNPs/Au-nano-Dendroids/GO/ALP/BCIP (ALP wash out condition), (ii) SPCE/AuNPs/Au-nano-Dendroids/GO/anti-ALP/BCIP, and (iii) SPCE/AuNPs/Au-nano-Dendroids/GO/anti-ALP/ALP/BCIP, **(B)** Histogram showing the effective intensity values obtained using DIC technique, **(C)** dose dependent EIS responses of ALP (100-1000 U/L) at SPCE/AuNPs/Au-nano-Dendroids/GO/anti-ALP sensor probe, **(D)** calibration plot obtained from the dose dependent Nyquist plot.

Figure 5: **(A)** Interference study using the fabricated SPCE/AuNPs/Au-nano-Dendroids/GO/anti-ALP sensor probe, (B) comparative dose-dependent detection of ALP in blood serum and PBS based on % recovery, (C) shows standard addition plot obtained for ALP detection in blood serum sample (5 times diluted) and (D) histogram showing the comparison of ALP levels detected using the sensor probe and clinically accepted method.

References:

Baranwal, A., Mahato, K., Srivastava, A., Maurya, P.K., Chandra, P., 2016. RSC Adv. 6(107), 105996-106010.

Berezhetska, O., Liberelle, B., De Crescenzo, G., Cicoira, F., 2015. J. Mater. Chem. B 3(25), 5087-5094.

Bodlaj, G., Hubmann, R., Saleh, K., Stojakovic, T., Biesenbach, G., Berg, J., 2010. World J. Gastroenterology 16(19), 2407-2410.

Buonaguro, F.M., Caposio, P., Tornesello, M.L., De Re, V., Franco, R., 2019. BioMed Res. International 2019.

Chandra, P., 2016. Nanobiosensors for personalized and onsite biomedical diagnosis. The Institution of Engineering and Technology.

Chandra, P., Tan, Y.N., Singh, S.P., 2017. Next generation point-of-care biomedical sensors technologies for cancer diagnosis. Springer.

Fu, L., Wu, K., Ji, J., Zhang, J., Guo, X., 2017. A highly sensitive disposable glucose biosensor based on platinum nanoflowers decorated screen printed carbon electrode, 2017 IEEE Sensors. pp. 1-3.

Hallaway, B.J., O'Kane, D.J., 2000. Chemiluminescence assay of serum alkaline phosphatase and phosphoprotein phosphatases, Methods in Enzymology. Academic Press, pp. 391-401.

Jiang, H., Islam, M.S., Sazawa, K., Hata, N., Taguchi, S., Nakamura, S., Sugawara, K., Kuramitz, H., 2016. Int. J. Electrochem. Sci. 11, 5090-5102.

Jimison, L.H., Hama, A., Strakosas, X., Armel, V., Khodagholy, D., Ismailova, E., Malliaras, G.G., Winther-Jensen, B., Owens, R.M., 2012. J. Mater. Chem. 22(37), 19498-19505.

Keshaviah, A., Dellapasqua, S., Rotmensz, N., Lindtner, J., Crivellari, D., Collins, J., Molleoni, M., Thürlimann, B., Mendiola, C., Aebi, S., Price, K., Pagani, O., Simoncini, E., Castiglione Gertsch, M., Gelber, R., Coates, A., Goldhirsch, A., 2007. Annals of Oncology 18(4), 701-708.

Kim, T.-I., Kim, H., Choi, Y., Kim, Y., 2011. Chem. Commun. 47(35), 9825-9827.

King, E., Delory, G., 1948. Postgraduate Med. J. 24(272), 299.

Lee, J.Y., Ahn, J.K., Park, K.S., Park, H.G., 2018. RSC Adv. 8(20), 11241-11246.

Mahato, K., Chandra, P., 2019. Biosens. Bioelectron. 128, 9-16.

Mahato, K., Nagpal, S., Shah, M.A., Srivastava, A., Maurya, P.K., Roy, S., Jaiswal, A., Singh, R., Chandra, P., 2019. 3 Biotech 9(2), 57.

McComb, R.B., Bowers, G.N., 1972. Clin. Chem. 18(2), 97-104.

Pei, H., Zhu, S., Yang, M., Kong, R., Zheng, Y., Qu, F., 2015. Biosens. Bioelectron. 74, 909-914.

Roy, S., Soin, N., Bajpai, R., Misra, D.S., McLaughlin, J.A., Roy, S.S., 2011. J. Mater. Chem 21(38), 14725-14731.

Ruan, C., Wang, W., Gu, B., 2006. Anal. Chem. 78(10), 3379-3384.

Takehana, K., Onomi, R., Hatate, K., Yamagishi, N., 2019. J. Vet. Med. Sci. 81(4), 551–554.

Valera, A.E., Nesbitt, N.T., Archibald, M.M., Naughton, M.J., Chiles, T.C., 2019. ACS Sensors 4(3), 654-659.

Wang, J.H., Wang, K., Bartling, B., Liu, C.-C., 2009. Sensors (Basel) 9(11), 8709-8721.

Wang, R., Liu, W.-D., Wang, A.-J., Xue, Y., Wu, L., Feng, J.-J., 2018. Biosens. Bioelectron 99, 458-463.

Xi, C., Jin, C., ZHANG, H.-Y., Fu-Bing, W., Fang-Fang, W., Xing-Hu, J., Zhi-Ke, H., 2016. Chinese J. Anal. Chem. 44(4), 591-596.

Zaaba, N.I., Foo, K.L., Hashim, U., Tan, S.J., Liu, W.-W., Voon, C.H., 2017. Procedia Engineering 184, 469-477.

Zhao, Y., Zheng, Y., Kong, R., Xia, L., Qu, F., 2016. Biosens. Bioelectron. 75, 383-388.

Zhao, Y., Zheng, Y., Zhao, C., You, J., Qu, F., 2015. Biosens. Bioelectron. 71, 200-206.

Sl. No.	Spiked ALP (U/L)	Recovered ALP (U/L)	% Recovery	% RSD
1	100	172.5 (±10.17)	172.5	5.9
2	200	279.3 (±12.10)	139.65	4.3
3	300	431.52 (±19.41)	143.84	4.5
4	400	527.9(±24.28)	131.97	4.6
5	500	646.72 (±28.42)	129.34	4.4
6	600	727.86 (±30.42)	121.31	4.2
7	700	777.4 (±31.87)	111.06	4.1
8	800	870.75(±37.44)	108.84	4.3
9	900	1015.58 (±51.79)	112.84	5.1
10	1000	1132.71(±44.17)	113.27	3.9

Table 1: The recovery table showing the spiked - recovered ALP concentrations, % recovery, and RSD values.

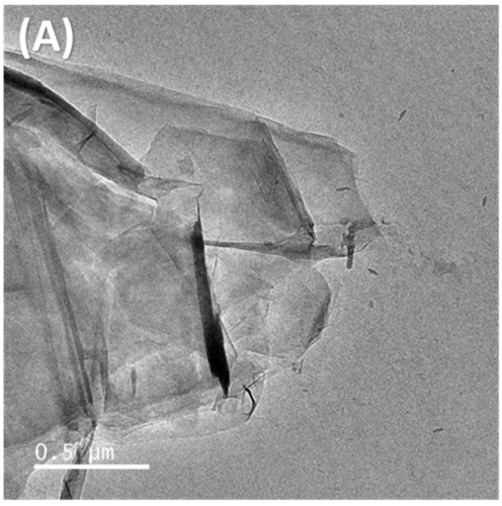
(A)
0.5 μm

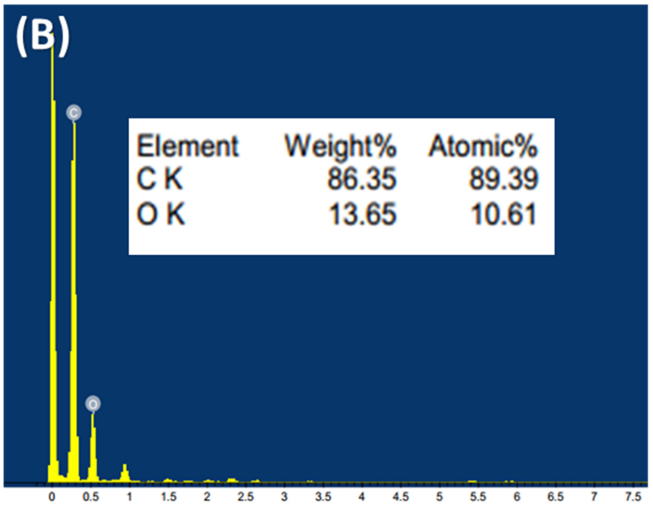
(B)
Element Weight% Atomic%
C K 86.35 89.39
O K 13.65 10.61
0 0.5 1 1.5 2 2.5 3 3.5 4 4.5 5 5.5 6 6.5 7 7.5

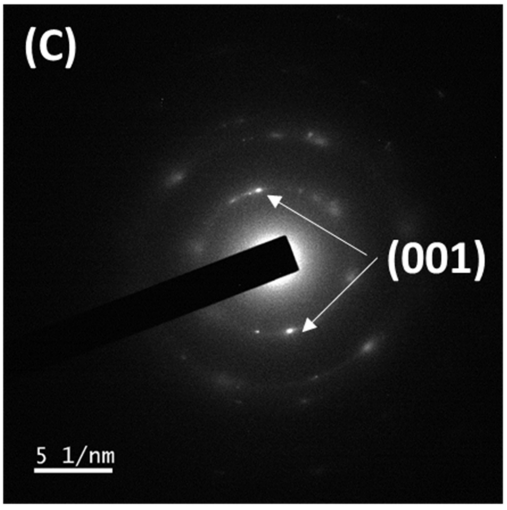
(C)
(001)
5 1/nm

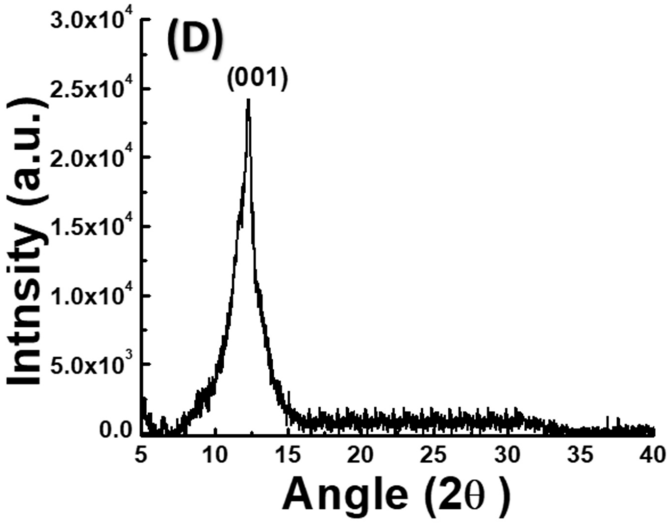
(D)
(001)
Intnsity (a.u.)
3.0x10^4
2.5x10^4
2.0x10^4
1.5x10^4
1.0x10^4
5.0x10^3
0.0
5 10 15 20 25 30 35 40
Angle (2θ)

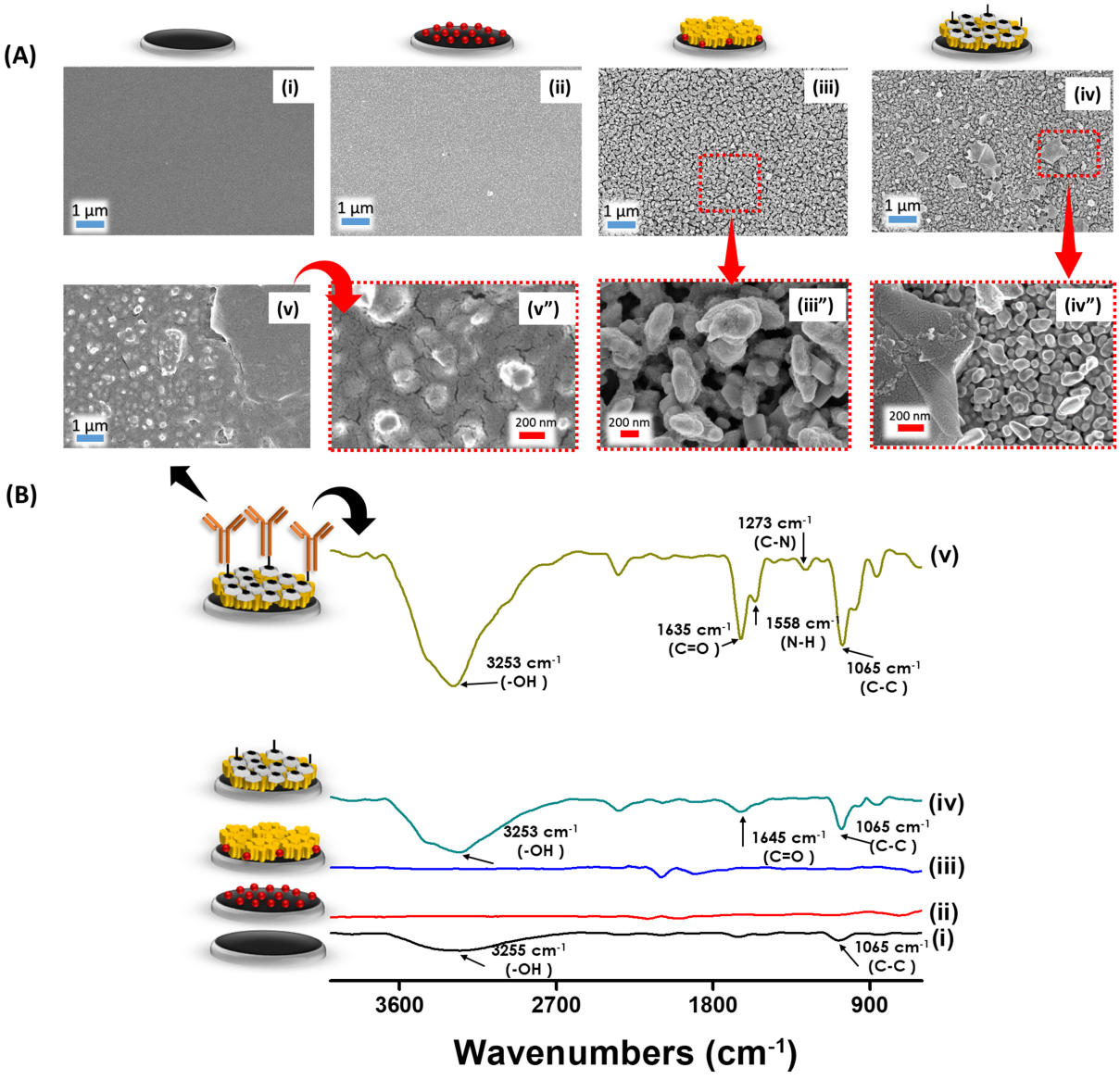
(A)
(i)
(ii)
(iii)
(iv)
(v)
(v")
(iii")
(iv")
1 µm
200 nm
(B)
1273 cm-1
(C-N)
(v)
1635 cm-1
(C=O)
1558 cm-1
(N-H)
3253 cm-1
(-OH)
1065 cm-1
(C-C)
(iv)
3253 cm-1
(-OH)
1645 cm-1
(C=O)
1065 cm-1
(C-C)
(iii)
(ii)
(i)
3255 cm-1
(-OH)
1065 cm-1
(C-C)
3600
2700
1800
900
Wavenumbers (cm-1)

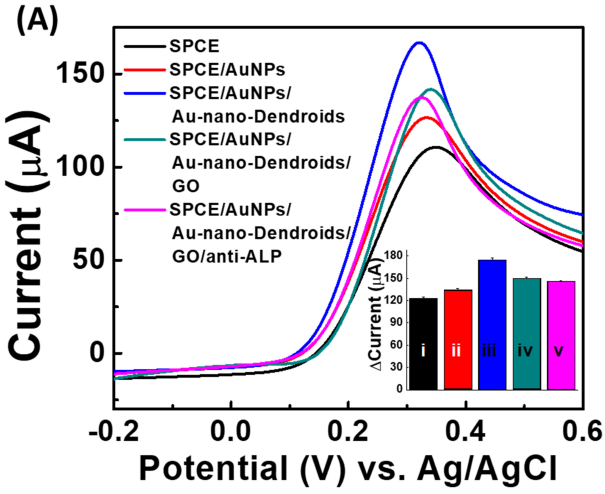
(A)
SPCE
SPCE/AuNPs
SPCE/AuNPs/
Au-nano-Dendroids
SPCE/AuNPs/
Au-nano-Dendroids/
GO
SPCE/AuNPs/
Au-nano-Dendroids/
GO/anti-ALP
Current (μA)
Potential (V) vs. Ag/AgCl
ΔCurrent (μA)
i
ii
iii
iv
v

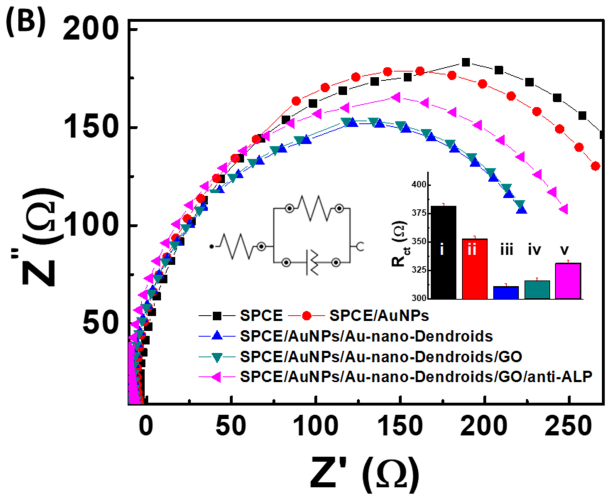
(B)
Z'' (Ω)
Z' (Ω)
SPCE
SPCE/AuNPs
SPCE/AuNPs/Au-nano-Dendroids
SPCE/AuNPs/Au-nano-Dendroids/GO
SPCE/AuNPs/Au-nano-Dendroids/GO/anti-ALP
R_ct (Ω)
i
ii
iii
iv
v

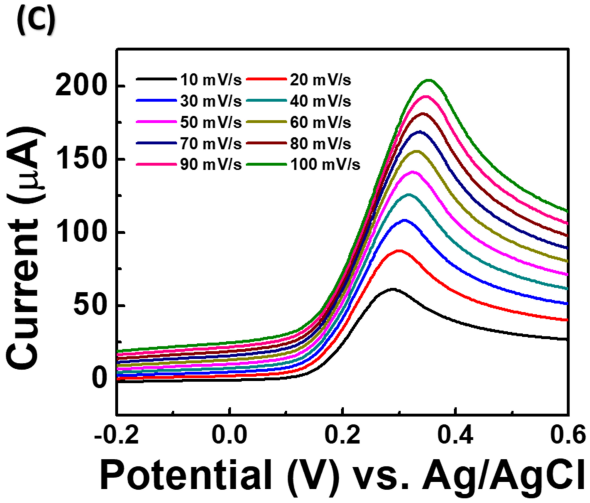
(C)
10 mV/s
20 mV/s
30 mV/s
40 mV/s
50 mV/s
60 mV/s
70 mV/s
80 mV/s
90 mV/s
100 mV/s
Current (μA)
Potential (V) vs. Ag/AgCl

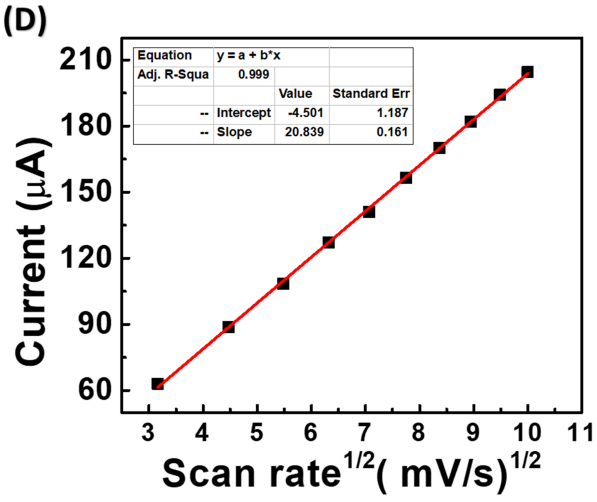
(D)
Equation y = a + b*x
Adj. R-Squa 0.999
Value Standard Err
-- Intercept -4.501 1.187
-- Slope 20.839 0.161
Current (μA)
Scan rate^1/2 (mV/s)^1/2

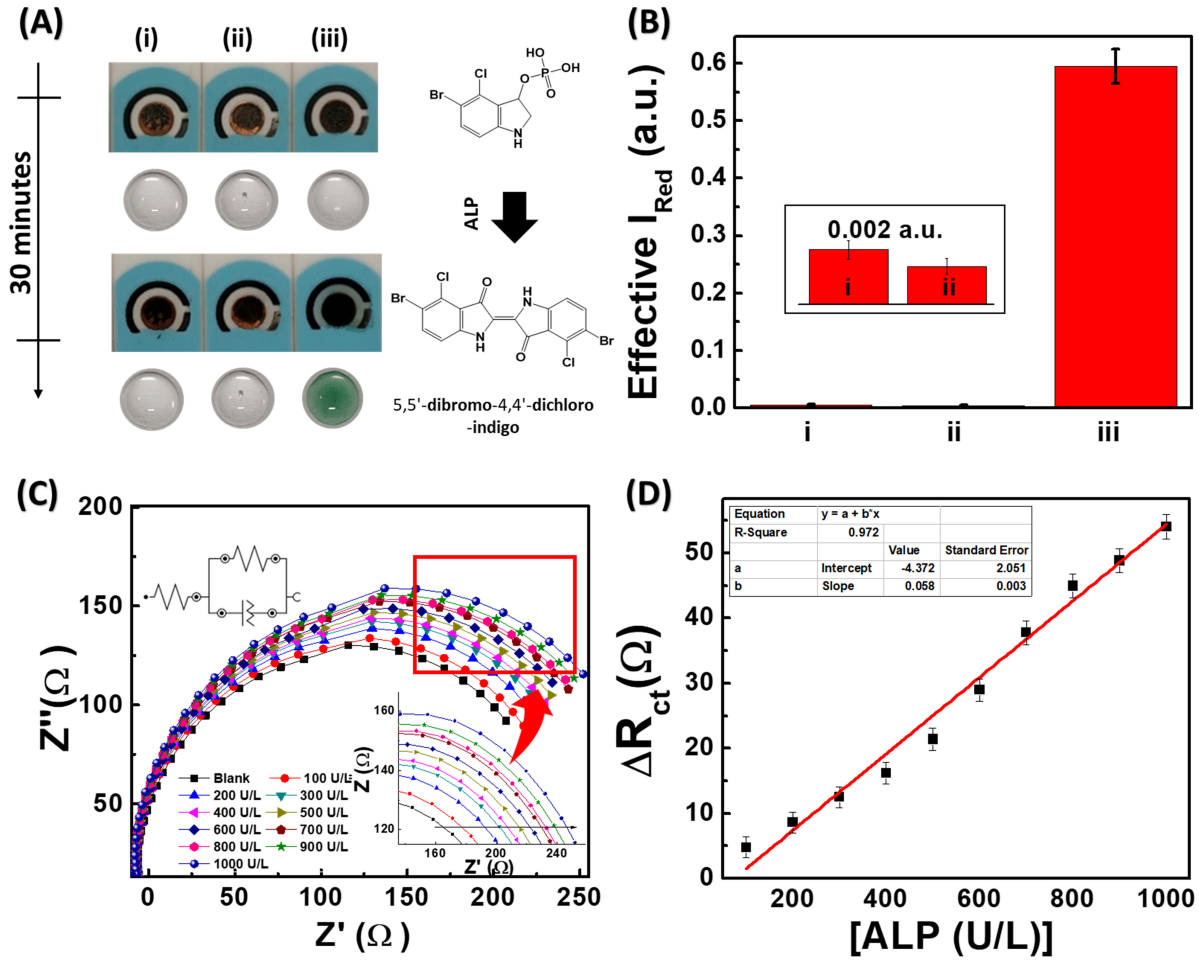
(A)
(i)
(ii)
(iii)
30 minutes
ALP
5,5'-dibromo-4,4'-dichloro
-indigo
(B)
Effective I_{Red} (a.u.)
0.002 a.u.
i
ii
iii
(C)
Z''(Ω)
Z' (Ω)
Blank
100 U/L
200 U/L
300 U/L
400 U/L
500 U/L
600 U/L
700 U/L
800 U/L
900 U/L
1000 U/L
(D)
ΔR_{ct} (Ω)
[ALP (U/L)]
Equation y = a + b*x
R-Square 0.972
Value Standard Error
a Intercept -4.372 2.051
b Slope 0.058 0.003

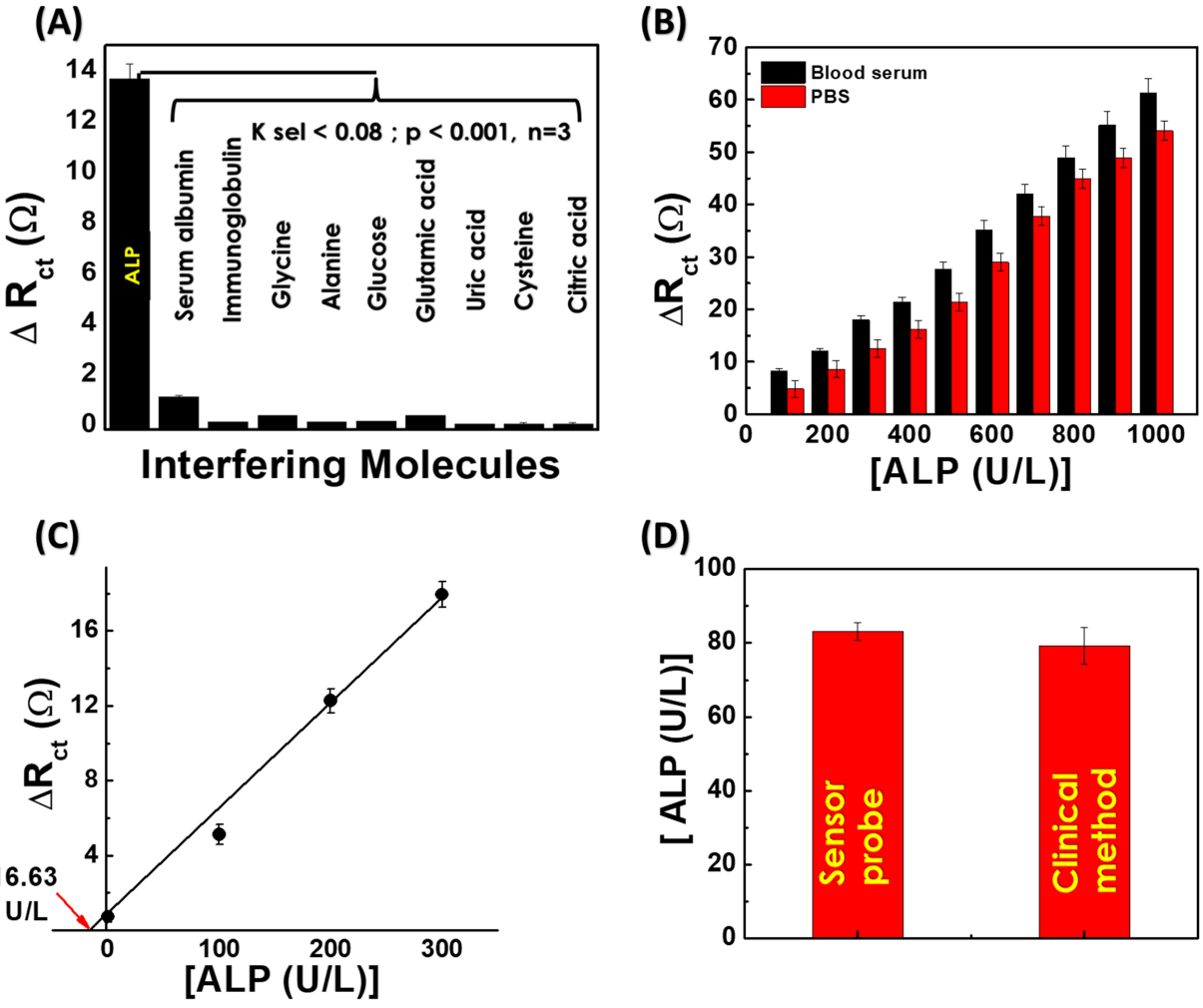
(A)
Δ R_ct (Ω)
ALP
Serum albumin
Immunoglobulin
Glycine
Alanine
Glucose
Glutamic acid
Uric acid
Cysteine
Citric acid
K sel < 0.08 ; p < 0.001, n=3
Interfering Molecules
(B)
ΔR_ct (Ω)
Blood serum
PBS
[ALP (U/L)]
(C)
ΔR_ct (Ω)
16.63
U/L
[ALP (U/L)]
(D)
[ALP (U/L)]
Sensor probe
Clinical method

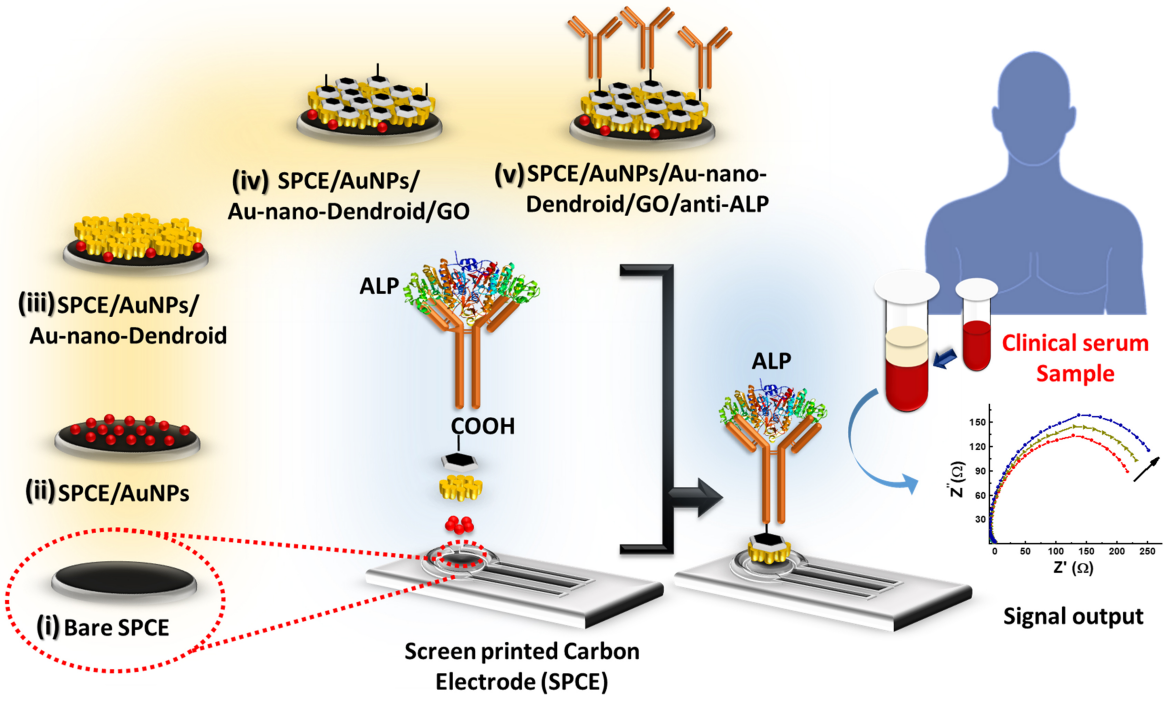

Highlights

- Label-free sensor for the estimation of alkaline phosphatase (ALP) in blood serum
- Developed sensor is able to detect serum ALP in clinical range
- First impedimetric determination of ALP using Au-nano-Dendroids and GO nanocomposites

Declaration of interests

☒ The authors declare that they have no known competing financial interests or personal relationships that could have appeared to influence the work reported in this paper.

☐The authors declare the following financial interests/personal relationships which may be considered as potential competing interests: